催化学报
2012 Chinese Journal of Catalysis Vol. 33 No. 1

文章编号: 0253-9837(2012)01-0140-13 国际版 DOI: 10.1016/S1872-2067(10)60283-5 研究论文: 140~151

$(NH_4)_2SiF_6$ 预处理改善 SBA-15 介孔材料的水热稳定性

宋明娟, 邹成龙, 牛国兴*, 赵东元

复旦大学化学系, 上海 200433

摘要: $(NH_4)_2SiF_6$ 预处理可对 SBA-15 介孔材料的表面缺陷进行补硅修正以及表面疏水化, 从而明显改善 SBA-15 材料的水热稳定性. 结果表明, 用摩尔分数为 5% 的 $(NH_4)_2SiF_6$ 水溶液, 按引入 1% 的 SiO_2 计量对 SBA-15 进行处理后, 其水热稳定性明显改善, 在 100 °C 沸水中处理 14 d, 或在 800 °C 下用 100% 水蒸气处理 12 h 后, 均保持较好的介观有序度、形貌及六方孔道结构, 比表面积分别高达 310 和 213 m^2/g, 但 $(NH_4)_2SiF_6$ 处理量过高, SBA-15 水热稳定性反而下降.

关键词: 水热稳定性; 氟硅酸铵; SBA-15 分子筛; 介孔材料; 补硅; 疏水化

中图分类号: O643 **文献标识码**: A

收稿日期: 2011-08-01. 接受日期: 2011-09-13.

*通讯联系人. 电话: (021)51630205; 传真: (021)51630307; 电子信箱: gxniu@fudan.edu.cn

基金来源: 国家自然科学基金 (20890123); 国家重点基础研究发展计划 (973 计划, 2010CB226901).

本文的英文电子版(国际版)由Elsevier出版社在ScienceDirect上出版(http://www.sciencedirect.com/science/journal/18722067).

Improving the Hydrothermal Stability of Mesoporous Silica SBA-15 by Pre-treatment with $(NH_4)_2SiF_6$

SONG Mingjuan, ZOU Chenglong, NIU Guoxing*, ZHAO Dongyuan

Department of Chemistry, Fudan University, Shanghai 200433, China

Abstract: The hydrothermal stability of the mesoporous silica material SBA-15 was improved by a pre-treatment of 5 mol% ammonium hexafluorosilicate solution with 1 mol% SiO_2 ratio of $(NH_4)_2SiF_6$ and SBA-15. The modified SBA-15 kept its ordered meso-structure well even when kept under boiling water for 14 d or 100 % H_2O stream at 800 °C for 12 h, and still had BET surface areas as high as 310 and 213 m^2/g, respectively, after these treatments. The possible reasons for the stabilization were that the surface defects of SBA-15 were partially repaired by silicon insertion and some silicon hydroxyls were replaced by F^- ions. Larger amounts of ammonium hexafluorosilicate did not give more stabilization.

Key words: hydrothermal stability; ammonium fluorosilicate; SBA-15 zeolite; mesoporous material; silicon insertion; hydrophobization

Received 1 August 2011. Accepted 13 September 2011.

**Corresponding author. Tel: +86-21-51630205; Fax: +86-21-51630307; E-mail: gxniu@fudan.edu.cn*

This work was supported by the National Natural Science Foundation of China (20890123) and the National Basic Research Program of China (973 Program, 2010CB226901).

English edition available online at Elsevier ScienceDirect (http://www.sciencedirect.com/science/journal/18722067).

介孔氧化硅 SBA-15 分子筛自问世以来, 因其孔道结构规整, 比表面积较大, 热和水热稳定性较高而广泛应用于催化、生物、医药、吸附分离等领域[1~10]. 但是, SBA-15 分子筛用作工业催化剂或载体时, 其水热稳定性仍偏低[11]. 因此, 通过各种手段提高介孔 SBA-15 的水热稳定性已成为当前该领域的研究热点之一[12~16].

利用"盐效应", 即在合成过程中引入 NaCl, NaF 和 EDTA 等盐类, 增加介孔材料的孔壁厚度[17,18]; 或严格控制晶化过程的 pH 值, 或进行二次晶化重构, 或引入杂原子至介孔骨架, 保证介孔材料孔壁的有效交联[19~26]; 或通过硅烷基化处理或氟离子取代

将材料表面疏水化[27,28]等手段, 均在不同程度上改善了 SBA-15 分子筛的水热稳定性. 但这些方法或多或少存在操作复杂、条件苛刻、控制困难以及耗时耗能等不足. 因此, 从应用角度出发, 寻求一种简单低能耗的改良方法已成为当务之急.

氟硅酸铵 $(NH_4)_2SiF_6$ 是 HY 或 HZSM-5 等微孔分子筛常用的脱铝试剂. 它通过同晶取代可及时补硅, 修复分子筛脱铝过程产生的晶体缺陷, 保障分子筛结构稳定. 采用 $(NH_4)_2SiF_6$ 处理可望修补介孔材料的表面缺陷, 同时其分解产生的氟离子可取代介孔材料表面的硅羟基, 增加介孔材料的疏水化程度, 以减少水分子对其刻蚀, 从而提高 SBA-15 分子筛的水热稳定性. 但目前有关这方面工作的报道却很少.

本文采用不同 $(NH_4)_2SiF_6$ 用量预处理 SBA-15 分子筛, 研究了它在 100 °C 沸水和 800 °C, 100 % 水蒸气中耐水热稳定的变化规律, 并讨论了 $(NH_4)_2SiF_6$ 的作用机理.

1 实验部分

1.1 样品的制备

SBA-15 分子筛按文献[3]合成. 在 38 °C 下, 将 20 g 嵌段共聚物表面活性剂 P123 ($EO_{20}PO_{70}EO_{20}$, M_w = 5800, Aldrich) 溶于 750 ml 盐酸溶液 (2 mol/L) 中, 加入 42 g 正硅酸乙酯 (TEOS, 分析纯) 搅拌 20 h. 将上述溶液转移至水热釜中, 在 100 °C 晶化 48 h. 经抽滤、洗涤和干燥后, 在 550 °C 焙烧 5 h, 所得白色粉末即为 SBA-15 样品.

将 10 g 所制 SBA-15 样品置于 300 ml 的 NH_4Ac 溶液 (0.3 mol/L) 中, 在 60 °C 缓慢滴加不同质量的 5 mol% $(NH_4)_2SiF_6$ 或 NH_4F 溶液. 滴加完毕后, 搅拌反应 1 h, 再抽滤、洗涤和烘干. $(NH_4)_2SiF_6$ 改性的样品分别标记为 S-*X*, 其中 *X* 表示 $(NH_4)_2SiF_6$ 引入的 SiO_2 与 SBA-15 中 SiO_2 的摩尔比. NH_4F 改性的样品分别标记为 F-*X*, 其中 *X* 表示 NH_4F 引入的 F^- 离子数与对应 $(NH_4)_2SiF_6$ 用量为 *X* 时引入的 F^- 离子数相同.

1.2 样品的水热稳定性评价

将氟硅酸铵处理的 SBA-15 样品装入盛有蒸馏水的水热反应釜中, 密闭置于 100 °C, 分别放置 7 和 14 d, 样品分别标记为 S-*X*-7 和 S-*X*-14; 未经氟硅酸铵处理的 SBA-15 相应样品分别记为 SBA-15-7 和 SBA-15-14.

将氟硅酸铵处理后的样品 S-0.01 放入管式炉, 升温至 800 °C, 通入 100 % 水蒸气, 分别处理 3, 6, 12 和 24 h. 所得样品标记为 S-0.01-800-*t*, 其中 *t* 为水热处理时间 (h).

1.3 样品的表征

X 射线衍射 (XRD) 谱由 Bruker D4 型粉末衍射仪测定, Cu K_α射线源, 管压 40 kV, 管流 40 mA. N_2 吸附-脱附等温线在 Micromeritics Tristar 3020 型分析仪上于 –196 °C 下测定. BET 法计算样品的比表面积, BJH 法计算孔径分布, 孔体积根据相对压力为 0.995 处的吸附计算得到, 微孔利用 *t*-plot 方法进行分析. 透射电镜 (TEM) 测试在 JEOL 2011 型电镜上进行, 工作电压 200 kV. 扫描电镜 (SEM) 测试在 Philip XL 30 型电镜上进行, 工作电压 20 kV. FT-IR 谱在 Nicolet FT-IR Avater 360 型仪器上测定. 测量前, 自支持样品须在 450 °C, 1.0×10^{-4} Pa 真空度下预处理 5 h. ^{29}Si 核磁共振在德国 Bruker DSX-300 型仪器上完成. 共振频率 59.627 MHz, 射频场强度 50 kHz, 脉冲宽度 2.5 μs, 采样次数 1800.

2 结果与讨论

2.1 沸水条件下样品的稳定性

图 1 为 SBA-15 和 S-0.01 样品的 XRD 谱. 可以看出, 未经处理的 SBA-15 样品在 2θ = 0.9° 和

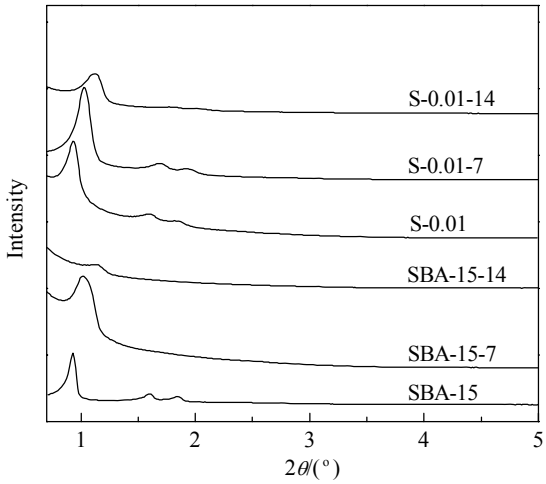

图 1 SBA-15 和 S-0.01 样品经沸水处理不同时间后的 XRD 谱

Fig. 1. XRD patterns of SBA-15 and S-0.01 samples treated under boiling water for different time.

1.5°~2.0° 处清晰出现 3 个分别归属于六方 (空间群 *p6mm*) 结构 (100), (110) 和 (200) 晶面的衍射峰, 说明该材料具有规整的六方相介观结构. 该样品经 100 °C 沸水处理 7 d 后, 其 (100) 晶面的衍射峰仍清晰可见, 但其 (110) 和 (200) 晶面的衍射峰完全消失. 处理 14 d 后, 其 (100) 面的衍射峰也基本消失. 这说明未改性的 SBA-15 材料经 100 °C 处理 7 d 和 14 d, 其二维六方结构的有序性基本丧失.

经 $(NH_4)_2SiF_6$ 处理的 S-0.01 样品, 经 100 °C 沸水处理 7 d 后, 材料依然出现 (100), (110) 和 (200) 晶面的衍射峰, 只是其位置向高角度方向移动. 这说明在水热过程中, SBA-15 材料的晶胞发生了收缩, 但仍很好地保持了六方结构有序度; 当处理 14 d 后, 样品 (100), (110) 和 (200) 晶面的衍射峰仍清晰可辨, 只是强度有所下降. 由此可见, 经 $(NH_4)_2SiF_6$ 处理后, SBA-15 介孔分子筛的水热稳定性明显改善.

图 2 为 SBA-15 和 S-0.01 样品的 N_2 吸附-脱附等温线. 由图可见, 未改性的 SBA-15 介孔材料具有典型的 H1 型滞后环; 经 100 °C 水热处理 7 d 和 14 d 后, 其 H1 型滞后环完全消失, 比表面积也从 644 m^2/g 分别下降至 176 和 107 m^2/g, 最可几孔径也从 8.5 nm 降至 5.5 nm 左右 (见表 1).

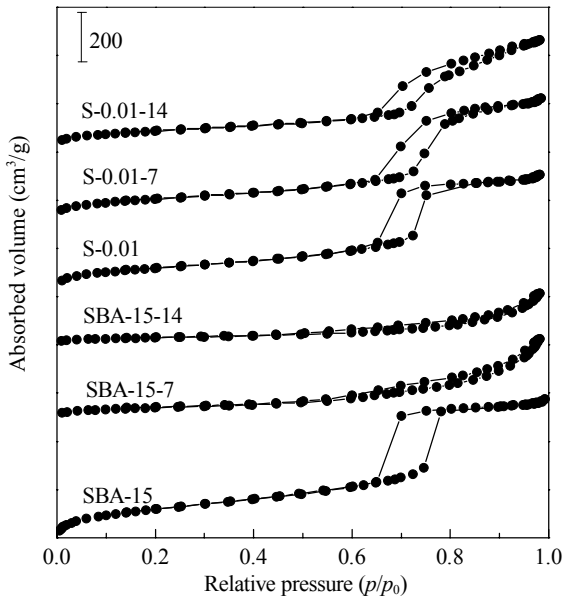

图 2 SBA-15 和 S-0.01 样品经沸水处理不同时间后的低温 N_2 吸附-脱附等温线

Fig. 2. N_2 adsorption-desorption isotherms of SBA-15 and S-0.01 samples treated under boiling water for different time.

表 1 SBA-15 和 S-0.01 样品经沸水处理不同时间后的孔结构参数

Table 1 Pore structural parameters of SBA-15 and S-0.01 samples after treatment with boiling water for different time

Sample	A_{BET}/(m^2/g)	A_{micro}/(m^2/g)	V/(cm^3/g)	V_t/(cm^3/g)	D/nm
SBA-15	644	80	0.98	0.03	8.5
SBA-15-7	176	22	0.52	0.008	5.4
SBA-15-14	107	18	0.33	0.007	5.5
S-0.01	424	55	0.78	0.02	7.7
S-0.01-7	375	53	0.81	0.02	7.7
S-0.01-14	310	44	0.72	0.02	7.8

经 100 °C 水热处理后, S-0.01 样品的 H1 型滞后环完整地保持, 说明 $(NH_4)_2SiF_6$ 处理不会影响其介观结构, 但比表面积降至 424 m^2/g. 其最可几孔径略降至 7.7 nm. 由图 1 可知, SBA-15 和 S-0.01 样品 (100) 晶面的衍射峰位置相同, 表明它们具有相同的晶胞参数. 因此, S-0.01 样品最可几孔径减小意味着 $(NH_4)_2SiF_6$ 的处理增加了其孔壁厚度. 这些未参与骨架修补的硅源由于堵住部分孔道或孔径减小是 S-0.01 样品比表面积小于未改性 SBA-15 的原因之一.

经 100 °C 沸水处理 7 d 后, S-0.01-7 样品仍具有典型的 H1 型滞后环, 其比表面积略下降为 375 m^2/g; 处理 14 d 的 S-0.01-14 样品的滞后环略有变形, 在 p/p_0 较窄的范围 (0.65~0.75) 内出现类似 H1 滞后环, 吸附容量随分压改变有明显的突越变化, 说明它依然存在一定的介孔; 但其滞后环闭合点延伸至 $p/p_0 = 1.0$, 表明水热处理已导致部分介孔丧失, 孔径增大. 尽管如此, S-0.01-14 样品的比表面积仍达 310 m^2/g, 远远大于未经 $(NH_4)_2SiF_6$ 改性的 SBA-15-14 样品 (107 m^2/g). 这与 XRD 结果一致, 说明 $(NH_4)_2SiF_6$ 处理可显著提高 SBA-15 分子筛在沸水中的稳定性.

由表 1 和图 1 可见, S-0.01 样品与 S-0.01-7 及 S-0.01-14 样品具有相同的最可几孔径; 但 (100), (110) 和 (200) 晶面的衍射峰随沸水处理时间的延长而向高角度位移, 说明沸水处理会引起 SBA-15 的孔壁逐渐收缩.

图 3 为 SBA-15 和 S-0.01 样品的 SEM 照片. 可以看出, 未改性的 SBA-15 材料具有麦穗状形貌. 经 100 °C 沸水处理 7 d 后, 原本排列有序的短棒结构开始散乱; 水热处理 14 d 后, 这种短棒分散、解离

的现象尤为明显. 而 S-0.01 样品在 100 °C 沸水中处理 7 和 14 d 后, 依然很好地保持了原先的麦穗状. 这再次表明 $(NH_4)_2SiF_6$ 处理提高了 SBA-15 的水热稳定性.

图 4 为 SBA-15 和 S-0.01 样品的 TEM 照片. 由图可以看出, 在 100 °C 沸水中处理 7 和 14 d 后, SBA-15 样品的介孔结构由最初的高度有序渐变为无序; 而 S-0.01 样品即使在 100 °C 水热处理 14 d, 其有序孔道结构依然清晰可辨. 这与上文结果是一致的.

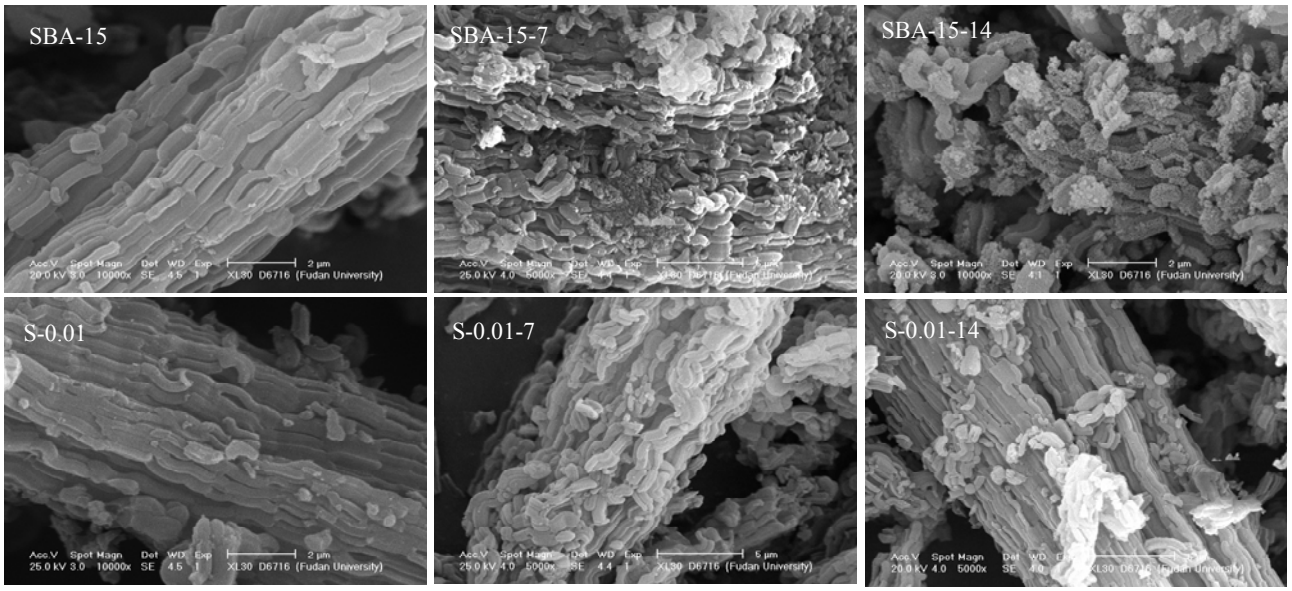

图 3 SBA-15 和 S-0.01 样品经沸水处理不同时间后的 SEM 照片

Fig. 3. SEM images of SBA-15 and S-0.01 samples after treatment with boiling water for different time.

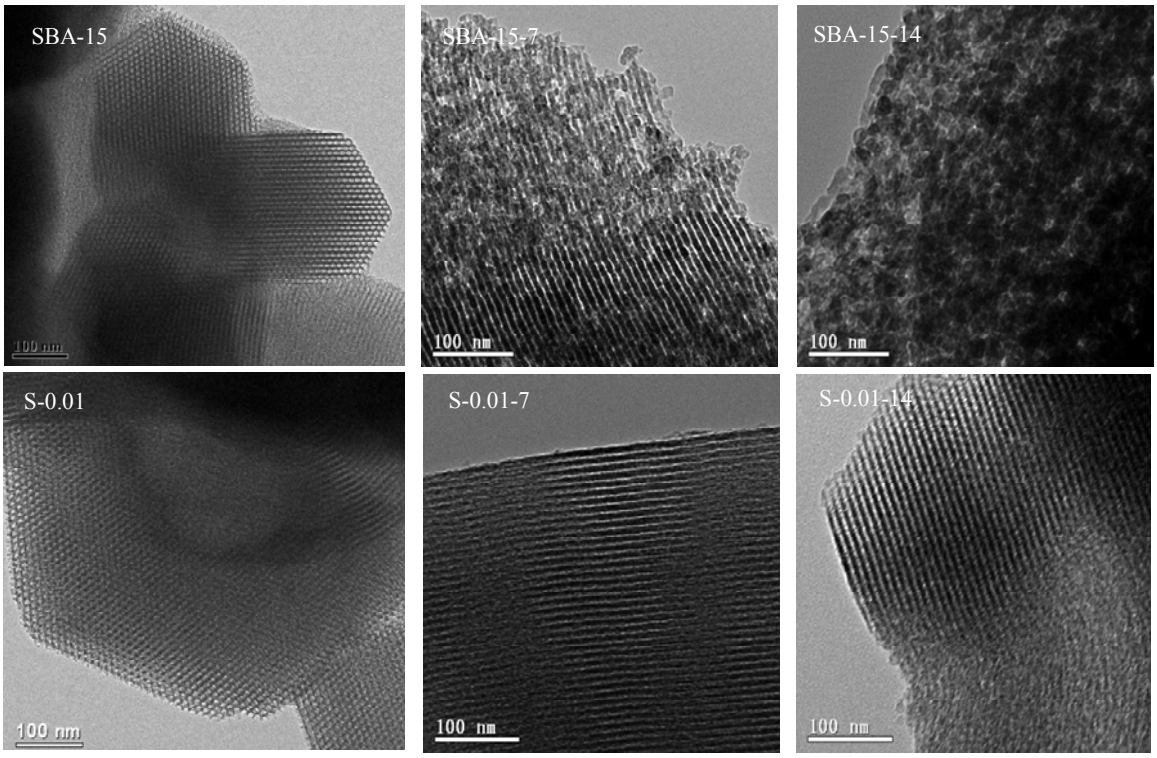

图 4 SBA-15 和 S-0.01 样品经沸水处理不同时间后的 TEM 照片

Fig. 4. TEM images of SBA-15 and S-0.01 samples after treatment with boiling water for different time.

2.2 水蒸气条件下样品的稳定性

为了进一步考察 $(NH_4)_2SiF_6$ 处理对 SAB-15 水热稳定性的影响, 本文考察了 S-0.01 样品在 800 °C, 100% 水蒸气下处理不同时间后的稳定性.

图 5 和图 6 分别为各样品的 X 射线小角衍射 (SAXS) 谱和 N_2 吸附-脱附等温线. 可以发现, 高温水蒸气处理 12 h 之内, S-0.01 样品均呈现清晰的 (100), (110) 和 (200) 晶面的衍射峰及扭变的 H1 滞后环, 说明 S-0.01 样品仍能保持较好有序的介孔. 当处理 24 h 后, 这些有序介孔基本消失.

各样品的 TEM 照片 (见图 7) 也证实了这一点, 即高温水蒸气在处理 12 h 之前, 样品很好地保持了规整的孔道结构; 达 24 h 时, 介观结构则已完全被破坏.

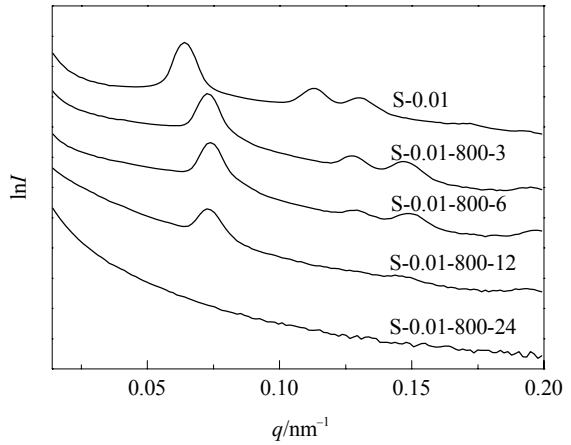

图 5 800 °C 水热处理不同时间后 S-0.01 样品的 SAXS 谱

Fig. 5. SAXS patterns of S-0.01 samples treated with 100% H_2O stream at 800 °C for different time.

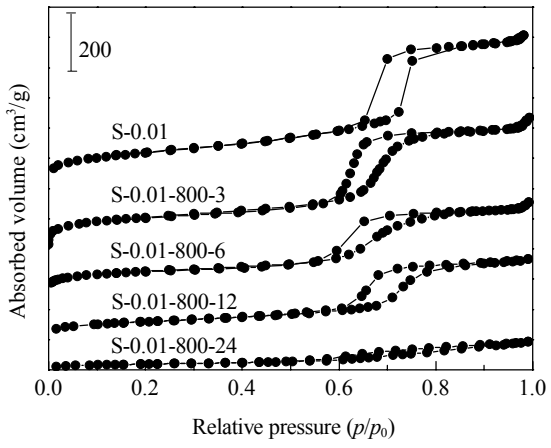

图 6 800 °C 水热处理不同时间后 S-0.01 样品的 N_2 吸附-脱附等温线

Fig. 6. N_2 adsorption-desorption isotherms of S-0.01 samples treated with 100% H_2O stream at 800 °C for different time.

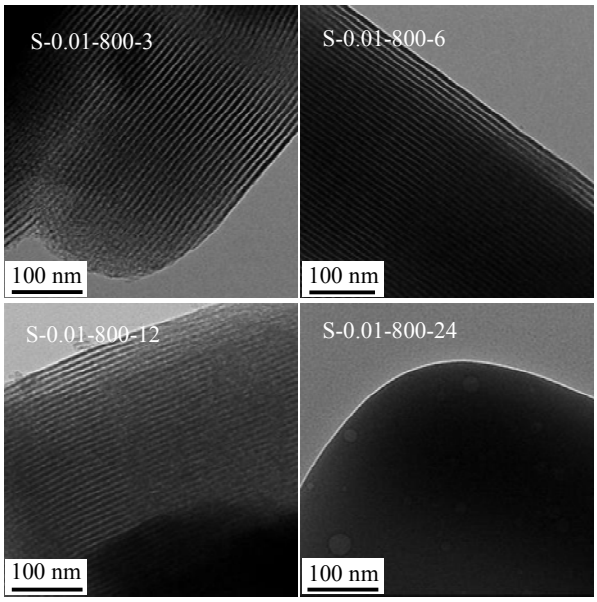

图 7 800 °C 水热处理不同时间后 S-0.01 样品的 TEM 照片

Fig. 7. TEM images of S-0.01 samples treated with 100% H_2O stream at 800 °C for different time.

将 800 °C 时水热处理时间与样品的比表面积作图, 结果示于图 8. 可以发现, 未经改性的 SBA-15 样品在 800 °C 水热初期 (< 6 h), 其比表面积随水热时间的延长而急速下降, 至 6 h 后趋于平缓. 这说明 SBA-15 材料的结构在 800 °C 水热处理 6 h 即可遭破坏. 尽管 S-0.01 样品的初始比表面积有所减小, 但随水热时间的延长却呈线性缓慢降低, 且 3 h 后其比表面积均大于 SBA-15 样品. 这说明 $(NH_4)_2SiF_6$ 处理可以防止水热过程中 SBA-15 材料

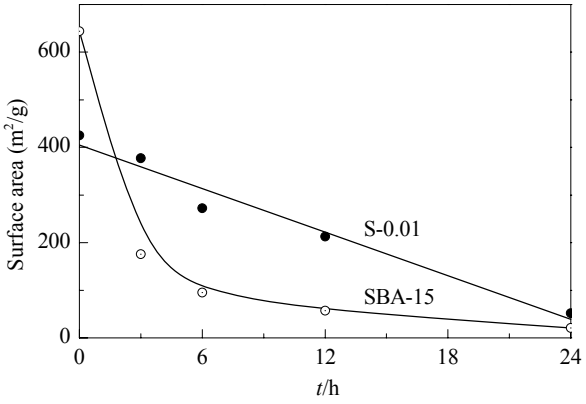

图 8 样品的比表面积与 800 °C 水热处理时间的关系

Fig. 8. BET surface areas as a function of the hydrothermal treatment time with 100% H_2O stream at 800 °C.

“雪崩式”的结构崩塌; 其有序结构的缓慢丧失是水热稳定性得到改善的重要原因之一.

2.3 $(NH_4)_2SiF_6$ 用量的影响

综上可见, 少量 $(NH_4)_2SiF_6$ 处理 (1% SiO_2 的引入量) 就可明显提高 SBA-15 材料的水热稳定性. 表 2 为经不同用量 $(NH_4)_2SiF_6$ 处理的 SBA-15 样品经 100 °C 沸水处理 7 和 14 d 后的比表面积. 由表可见, 随着 $(NH_4)_2SiF_6$ 用量的增加, SBA-15 样品的初始比表面积均有所减小, 基本维持在 420 m^2/g 左右, 说明 $(NH_4)_2SiF_6$ 用量对样品初始比表面积的影响较小. 但经沸水处理 7 和 14 d 后, 样品的比表面积随 $(NH_4)_2SiF_6$ 用量的增加反而减小, 说明 $(NH_4)_2SiF_6$ 用量增加并不能提高 SBA-15 材料的结构稳定性. 只有当其用量进一步增加至 12% 时, S-0.12 样品的水热稳定性又开始提高: 在 100 °C 水热处理 7 和 14 d 后, S-0.12 样品可维持其比表面积分别高达 357 和 326 m^2/g, 基本与 S-0.01 样品持平. $(NH_4)_2SiF_6$ 用量对 SBA-15 分子筛水热稳定性的影响与其同 SBA-15 的作用机理密切相关.

2.4 氟离子的影响

$(NH_4)_2SiF_6$ 处理 SBA-15 样品时, 必然会引入一定量的 F^-离子, 它在提高 SBA-15 材料水热稳定性中的贡献究竟如何? 由表 2 可见, 即使不用 $(NH_4)_2SiF_6$, 而用含相同 F^-离子含量的 NH_4F 溶液处理 SBA-15 材料后, F-*X* 系列样品的初始比表面积也与 S-*X* 样品一样大幅度减小. 这表明 F^-离子会对 SBA-15 的骨架进行“刻蚀”, 导致 S-*X* 和 F-*X* 系列样品的比表面积急剧减小.

其中, F-0.01 样品的初始比表面积与 S-0.01 样品的接近, 经 100 °C 沸水处理 7 和 14 d 后, 其比表面积分别降至 321 和 293 m^2/g, 小于 S-0.01 样品 (375 和 310 m^2/g), 但明显大于未经处理的 SBA-15 样品 (176 和 107 m^2/g). 这说明 F^-离子能改善 SBA-15 材料的水热稳定性, 与文献报道结果一致. 这主要是由于 F^-离子取代介孔材料表面的硅羟基形成 Si–F 后, 提高了其表面的疏水化程度, 增强了抵抗水分子侵蚀的能力[29~31]. Xu 等[32]用 ^{19}F NMR 证实 NH_4F 预处理 AlMCM-41 的过程中, 的确存在这种 F^-离子取代硅羟基的行为.

与 F-0.01 样品相比, S-0.01 样品的水热稳定性更高, 说明 $(NH_4)_2SiF_6$ 处理时, 除 F^-离子的疏水化作用外, Si 插入的协同作用也不可忽略.

经 100 °C 水热处理 7 和 14 d 后, F-*X* 样品的比表面积均随 NH_4F 用量的增加而减小, 说明氟化铵过多不利于提高 SBA-15 的水热稳定性; 而 S-*X* 样品的比表面积也随 $(NH_4)_2SiF_6$ 用量增加而减小, 只是用量达 12% 时, S-0.12 样品的水热稳定性却又明显提高. 这种异常也与 $(NH_4)_2SiF_6$ 的作用机理密切相关.

2.5 $(NH_4)_2SiF_6$ 的作用机理

图 9 为各 SBA-15 样品的 FT-IR 羟基谱. 由图可见, 经 $(NH_4)_2SiF_6$ 和 NH_4F 处理后, SBA-15 样品在 3734 cm^{-1} 处的羟基峰强度有所减弱, 而在 3667

表 2 不同量氟硅酸铵和氟化铵处理的样品经沸水处理不同时间后的比表面积

Table 2 BET surface areas of samples modified by the various amounts of $(NH_4)_2SiF_6$ and NH_4F after treatment with boiling water for different time

Sample	A_{BET}/(m^2/g)		
	0 d	7 d	14 d
S-0.01	424	375	310
S-0.02	406	271	220
S-0.04	472	275	247
S-0.08	413	165	181
S-0.12	419	357	326
F-0.01	416	321	293
F-0.02	424	280	255
F-0.04	402	210	222
F-0.08	378	268	176
F-0.12	377	116	142

F-*X* denotes that the number of F^- ions from NH_4F was the same as that from $(NH_4)_2SiF_6$ with the amount of *X*.

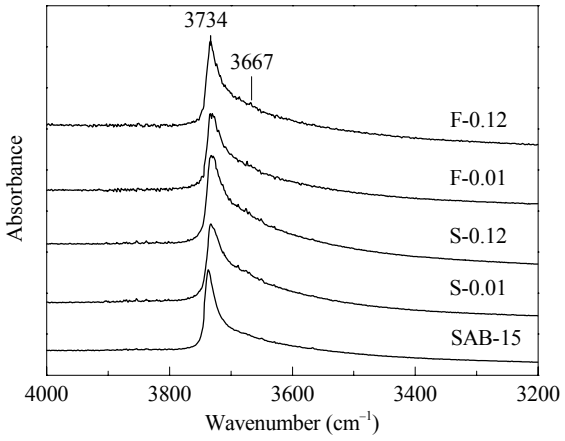

图 9 SBA-15, S-*X* 和 F-*X* 系列样品的 FT-IR 羟基谱

Fig. 9. FT-IR spectra of the hydroxyl region of the SBA-15, S-*X*, and F-*X* series samples.

cm^{-1} 处的硅羟基峰强度有所增强且宽化. 后者可归属于 MCM-41 表面受邻近基团氢键影响的硅羟基伸缩振动峰[33]. S-*X* 和 F-*X* 系列样品中, 部分表面硅羟基被 F^- 离子取代, 由于 F^- 电负性大于 OH^-, 导致与邻近硅羟基的氢键作用增强. 因此, 3667 cm^{-1} 峰略有增强.

还可以看出, S-*X* 系列样品的羟基谱与 F-*X* 样品的非常相似. 这说明 $(NH_4)_2SiF_6$ 处理时, 解离的 F^- 离子对 SBA-15 表面具有与 NH_4F 一样的作用效果; 且随着 F^- 离子量的增加, 两者羟基谱的变化均很小. 而如前所述, 既然 F^- 离子能取代硅羟基形成 Si–F 键, 则该羟基峰应该明显减小. 这种不一致性的原因可能为: (1) 与原位合成过程中引入 F^- 离子不同, 用预处理方式引入 F^- 时, F^- 离子可能主要是取代 SBA-15 表面的硅羟基, 却较难渗透至介孔壁内层取代体相中孤立的硅羟基, 而被 F^- 取代的表面硅羟基所占比例很少, 因而羟基谱变化很小; (2) F^- 离子刻蚀 SBA-15 骨架而形成新的 Q^3 结构 ($Si(OSi)_3OH$, 见下文) 和新的硅羟基, 从而抵消部分 F^- 离子的取代效应.

图 10 为 SBA-15, S-0.01 和 F-0.01 样品的 ^{29}Si NMR 谱. 可以看出, 三者在 $\delta = -101$ 和 -110 处均出现归属于 Q^3 和 Q^4 结构的 ^{29}Si 共振峰[34]. 其 Q^3/Q^4 比分别为 4.7%, 15.7% 和 19.8%. 可见, 经 $(NH_4)_2SiF_6$ 和 NH_4F 处理后, Q^3 峰明显增强. 这暗示含氟试剂处理 SBA-15 时, F^- 离子在取代 SBA-15 表面硅羟基形成疏水化表面的同时, 也会刻蚀 SBA-15 表面, 将 Q^4 的 $Si(OSi)_4$ 结构转变为 Q^3 的

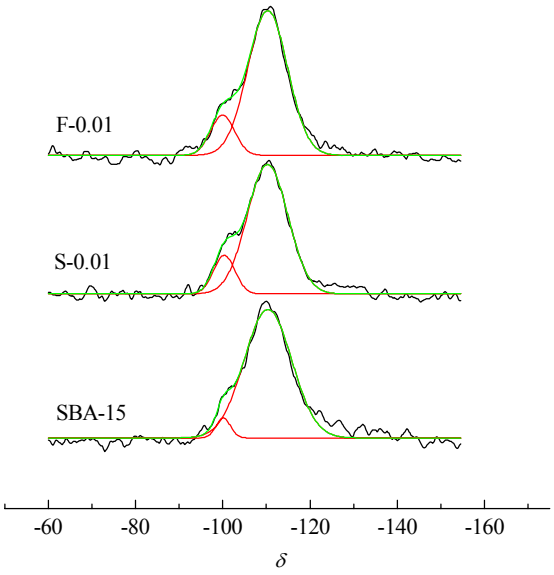

图 10 SBA-15, S-0.01 和 F-0.01 样品的 ^{29}Si NMR 谱

Fig. 10. ^{29}Si NMR spectra of SBA-15, S-0.01, and F-0.01 samples.

$Si(OSi)_3OH$ 结构.

比较 S-0.01 和 F-0.01 样品的 Q^3/Q^4 比可以发现, 虽然两者引入的 F^- 离子总量相同, 但前者的 Q^3/Q^4 比明显更低, 这说明采用 $(NH_4)_2SiF_6$ 处理 SBA-15 时, 有部分 Si 插入至 SBA-15 的表面缺陷中, 使部分 $Si(OSi)_3OH$ 结构转换成 $Si(OSi)_4$ 结构. 由此可见, $(NH_4)_2SiF_6$ 对 SBA-15 材料具有补硅和结构修补作用.

综上所述, $(NH_4)_2SiF_6$ 处理可提高 SBA-15 分子筛水热稳定性的作用机理可用图式 1 来描述. SBA-15 表面存在孤立的末端羟基和晶体缺陷, 当少

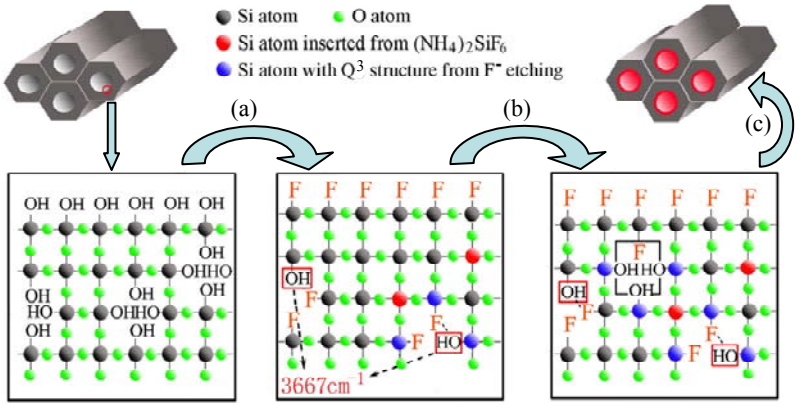

图式 1 氟硅酸铵与 SBA-15 分子筛的作用机理示意图

Scheme 1. Proposed mechanism showing the interaction between $(NH_4)_2SiF_6$ and SBA-15 zeolite.

量 $(NH_4)_2SiF_6$ 处理 SBA-15 时 (图示1(a)), Si 可以插入其表面缺陷位, 修补晶体结构, 使其趋于完整. 而 F^-离子在取代 SBA-15 表面末端羟基而形成疏水化表面的同时, 还刻蚀其表面, 形成新的 Q^3 晶体缺陷. 随着 $(NH_4)_2SiF_6$ 处理量的增加 (由 1% 增加至 12%, 图示 1(b)), 由于表面缺陷位已基本被 Si 占据, 增加的 Si 受空间位阻影响, 不能深入 SBA-15 的体相以修补其中的缺陷, 从而有效改善 SBA-15 的晶体结构以达到提高 SBA-15 的水热稳定性. 相反, $(NH_4)_2SiF_6$用量过多会导致体相中 F^-离子浓度增加, 加剧 F^-离子对 SBA-15 孔壁的刻蚀作用, 产生更多不饱和配位 Q^3 结构的 Si, 致使 SBA-15 的水热稳定性反而下降. 当 $(NH_4)_2SiF_6$ 处理量大于 12% 时 (图示 1(c)) , 由于 SiO_2 在 SBA-15 孔道内壁大量沉积, 形成比较致密的 SiO_2 保护膜, 阻止了水蒸气对 SBA-15 孔壁的侵蚀, 因而其水热稳定性又有所提高.

由上机理可知, $(NH_4)_2SiF_6$ 对 SBA-15 水热稳定性的改善程度取决于 Si 插入修补晶体缺陷和 F^-离子表面疏水化两者正效果与 F^-离子的刻蚀破坏负效果的总和. 尽管减少 F^-可提高样品的稳定性, 但 $(NH_4)_2SiF_6$ 分子中 F/Si 比是一定的, 这是本方法存在的主要问题之一.

尽管如此, 少量 $(NH_4)_2SiF_6$ 处理即可有效提高 SBA-15 的水热稳定性. 与其他方法相比, 该方法简单、廉价、能耗低, 且不引入杂原子等优点.

3 结论

少量 $(NH_4)_2SiF_6$ 改性可显著提高介孔 SBA-15 分子筛的水热稳定性. 在 100 °C 沸水中处理 14 d, 或在 800 °C, 100% 水蒸气中处理 12 h 后, 该样品仍保持较好的有序介观结构, 其比表面积分别高达 310 和 213 m^2/g, 远高于未改性样品. 这种改良方法简单、廉价、能耗低, 且不改变 SBA-15 材料的化学性质, 具有很好的实用价值.

参 考 文 献

1 Beck J S, Vartuli J C, Roth W J, Leonowicz M E, Kresge C T, Schmitt K D, Chu C T W, Olson D H, Sheppard E W, McCullen S B, Higgins J B, Schlenker J L. *J Am Chem Soc*, 1992, **114**: 10834

2 Kresge C T, Leonowicz M E, Roth W J, Vartuli J C, Beck J S. *Nature*, 1992, **359**: 710

3 Zhao D Y, Huo Q S, Feng J L, Chmelka B F, Stucky G D. *J Am Chem Soc*, 1998, **120**: 6024

4 Zhao D Y, Feng J L, Huo Q S, Melosh N, Fredrickson G H, Chmelka B F, Stucky G D. *Science*, 1998, **279**: 548

5 Bagshaw S A, Prouzet E, Pinnavaia T J. *Science*, 1995, **269**: 1242

6 Liu X Y, Tian B Z, Yu C Z, Gao F, Xie S H, Tu B, Che R C, Peng L M, Zhao D Y. *Angew Chem*, *Int Ed*, 2002, **41**: 3876

7 Yu C Z, Tian B Z, Fan B, Stucky G D, Zhao D Y. *Chem Commun*, 2001: 2726

8 Tanev P T, Chibwe M, Pinnavaia T J. *Nature*, 1994, **368**: 321

9 Tanev P T, Pinnavaia T J. *Science*, 1995, **267**: 865

10 张微, 徐恒泳, 毕亚东, 李文钊. 化工进展 (Zhang W, Xu H Y, Bi Y D, Li W Zh. *Chem Ind Eng Progr*), 2007, **26**: 152

11 Ryoo R, Jun S. *J Phys Chem B*, 1997, **101**: 317

12 Galarneau A, Nader M, Guenneau F, Renzo F D, Gedeon A. *J Phys Chem C*, 2007, **111**: 8268

13 Zhang F Q, Yan Y, Yang H F, Meng Y, Yu C Z, Tu B, Zhao D Y. *J Phys Chem B*, 2005, **109**: 8723

14 Han Y, Li N, Zhao L, Li D F, Xu X Z, Wu S, Di Y, Li C J, Zou Y C, Yu Y, Xiao F S. *J Phys Chem B*, 2003, **107**: 7551

15 Lai X Y, Tu J C, Wang H, Du J, Yang M, Mao D, Xing C J, Wang D, Li X T. *Chem Res Chin Univ*, 2009, **25**: 773

16 On D T, Kaliaguine S. *J Am Chem Soc*, 2003, **125**: 618

17 Chen G D, Wang L Z, Lei J Y, Zhang J L. *Microporous Mesoporous Mater*, 2009, **124**: 204

18 Li C L, Wang Y Q, Guo Y L, Liu X H, Guo Y, Zhang Z G, Wang Y S, Lu G Z. *Chem Mater*, 2007, **19**: 173

19 于善青, 赵瑞玉, 刘晨光. 石油学报 (石油加工)(Yu Sh Q, Zhao R Y, Liu Ch G. *Acta Petrol Sin (Petrol Process Sect)*), 2004, **20**(4): 79

20 Selvaraj M, Park D W, Ha C S. *Microporous Mesoporous Mater*, 2011, **138**: 94

21 Du Y C, Liu S, Zhang Y L, Nawaz F, Ji Y Y, Xiao F S. *Microporous Mesoporous Mater*, 2009, **121**: 185

22 Du Y C, Lan X J, Liu S, Ji Y Y, Zhang Y L, Zhang W P, Xiao F S. *Microporous Mesoporous Mater*, 2008, **112**: 225

23 Selvaraj M, Kawi S. *Chem Mater*, 2007, **19**: 509

24 Yang D J, Xu Y, Wu D, Sun Y H. *J Solid State Chem*, 2008, **181**: 2401

25 Ye F, Dong Z W, Zhang H J. *Mater Lett*, 2010, **64**: 1441

26 Song K, Guan J Q, Wang Z Q, Xu C, Kan Q B. *Appl Surf Sci*, 2009, **255**: 5843

27 Sun H, Tang Q H, Du Y, Liu X B, Chen Y, Yang Y H. *J Colloid Inter Sci*, 2009, **333**: 317

28 Wei J W, Shi J J, Pan H, Su Q F, Zhu J B, Shi Y. *Microporous Mesoporous Mater*, 2009, **117**: 596

29 Xia Q H, Hidajat K, Kawi S. *Mater Lett*, 2000, **42**: 102

30 Jiang T L, Tao H X, Ren J W, Liu X H, Wang Y Q, Lu G Z. *Microporous Mesoporous Mater*, 2011, **142**: 341

31 Chen G D, Wang L Z, Lei J Y, Zhang J L. *Microporous Mesoporous Mater*, 2009, **124**: 204

32 Xu M, Wang W, Seiler M, Buchholz A, Hunger M. *J Phys Chem B*, 2002, **106**: 3202

33 Chen J H, Li Q H, Xu R R, Xiao F S. *Angew Chem*, *Int Ed*,

1995, **34**: 2694
34 Sindorf D W, Maciel G E. *J Phys Chem*, 1982, **86**: 5208

英 译 文

English Text

Since its discovery in 1998, SBA-15 has attracted considerable attention as a potential catalyst support, adsorbent, hydrogen storage, and drug delivery media, and as a hard template for other nanostructure materials [1–10] because of its remarkably high thermal stability and variable pore size. However, the material has not been widely used in industry because of its relatively poor hydrothermal stability [11]. Under some extreme reaction conditions, such as the presence of steam at high temperature used for the regeneration of catalysts, it cannot maintain its meso-structure well enough. Therefore, there has been much work on the improvement of the hydrothermal stability of SBA-15 by various methods [12–16].

Many approaches have been employed, such as the thickening of the mesoporous wall by the addition of inorganic salts (such as KCl, NaCl, NaF, EDTA, etc.) during the preparation or by pre-hydrothermal treatment [17,18], promoting the degree of silica condensation in the pore walls by pH adjustment, secondary crystallization, and the incorporation of heteroatoms into the framework [19–26], and removing surface Si–OH groups by silylation and F^- ions [27,28]. These methods were successful for the synthesis of mesoporous SBA-15 material with good hydrothermal stability, but some of the methods were complex and their conditions were difficult to control, and some had high energy and time consumption. Therefore, it is urgent and challenging to develop a simple, facile, and cheap method to improve the hydrothermal stability of SBA-15 for practical applications.

Ammonium fluorosilicate ($(NH_4)_2SiF_6$) is a commonly used reagent in the dealumination of HY and HZSM-5 zeolites. The crystal defects of zeolites can be repaired by it by a successful incorporation of silicon to make the microporous framework of the zeolite stable in the process of dealumination. By using this feature, the surface defects of SBA-15 can be repaired as was done in zeolites. Also, surface Si–OH groups can be exchanged by F^- ions from the decomposition of ammonium fluorosilicate to form a hydrophobic surface, which can reduce the etching action of H_2O. Therefore, a potential approach to improve the hydrothermal stability of SBA-15 is by pre-treatment with $(NH_4)_2SiF_6$.

In this work, calcined SBA-15 was treated with various amounts of $(NH_4)_2SiF_6$ solution. The hydrothermal stability of the modified samples was investigated under boiling water or 100% H_2O stream at 800 °C for different time. The stabilization mechanism of $(NH_4)_2SiF_6$ was discussed based on characterization data from X-ray diffraction (XRD), N_2 absorption, ^{29}Si NMR, scanning electron microscopy (SEM), transmission electron microscopy (TEM), and Fourier transform infrared spectroscopy (FT-IR).

1 Experimental

1.1 Synthesis of samples

SBA-15 was synthesized first according to the procedure in Ref. [3]. A typical synthesis procedure was as follows. Triblock copolymer Pluronic (P123, $EO_{20}PO_{70}EO_{20}$, M_w = 5800, Aldrich, 20.0 g) was dissolved in 750 ml of 2 mol/L HCl solution at 38 °C. Then, tetraethyl orthosilicate (TEOS, 42.0 g) was added into the solution and hydrolyzed at 38 °C for 20 h under vigorous stirring. The mixture was transferred into a Teflon vessel, sealed, and heated at 100 °C for 48 h. The filtrated solid was washed, dried at 100 °C for 4 h, and calcined at 550 °C in air for 5 h to get the white powder SBA-15.

The calcined SBA-15 (10 g) was dispersed in 300 ml of 0.3 mol/L NH_4Ac solution. A measured amount of $(NH_4)_2SiF_6$ or NH_4F solution (5 mol%) was dropwise added under stirring at 60 °C. After 1 h, the filtrated solid was washed twice and dried at 100 °C for 4 h. The samples modified by $(NH_4)_2SiF_6$ were named as S-*X*, where *X* denoted the SiO_2 ratio of $(NH_4)_2SiF_6$ to SBA-15. The samples modified by NH_4F were named as F-*X*, where *X* here denoted that the number of F^- ions from NH_4F was the same as that from $(NH_4)_2SiF_6$ with the amount of *X*.

1.2 Evaluation of hydrothermal stability

SBA-15 samples were put in sealed Teflon vessels with some water, and heated at 100 °C for 7 d and 14 d, respectively. They were named as S-*X*-7 and S-*X*-14 for SBA-15 modified by $(NH_4)_2SiF_6$, and as SBA-15-7 and SBA-15-14 for unmodified SBA-15.

The S-0.01 sample was treated in a tube furnace under 100% H_2O stream at 800 °C for 3, 6, 12, and 24 h. They were named as S-0.01-800-*t*, where *t* means the time of the hydrothermal treatment.

1.3 Characterization of samples

XRD patterns were recorded on a German Bruker D4 X-ray diffractometer with Ni-filtered Cu K_α radiation (40 kV, 40 mA). Nitrogen adsorption-desorption isotherms were measured at –196 °C with a Micromeritics Tristar 3020 analyzer. The Brunauer-Emmett-Teller (BET) method was utilized to calculate the specific surface area, and the pore volume and pore size distributions were derived from the

adsorption branches of the isotherms using the Barrett-Joyner-Halenda (BJH) model. SEM was conducted on a Philip XL 30 electron microscope operated at 20 kV. TEM images were obtained with a JEOL 2011 microscope operated at 200 kV. ^{27}Si NMR spectra were recorded with a Bruker DSX-300 spectrometer. FT-IR spectra were recorded on a Nicolet FT-IR Avater 360. All samples were pre-treated at 450 °C in the vaccum of 1.0×10^{-4} Pa for 5 h.

2 Results and discussion

2.1 Hydrothermal stability under boiling water

The XRD result (Fig. 1) from the unmodified SBA-15 sample exhibited three well resolved peaks at $2\theta = 0.90^o$ and 1.5^o~2.0^o, corresponding to the (100), (110), and (200) diffraction peaks, which are the characteristics of the ordered structure of the 2D hexagonal space group (*p6mm*). After treatment under boiling water for 7 d, only the (100) diffraction peak appeared. The other peaks, (110) and (200), have disappeared. This result implied that the 2D hexagonal ordered structure of SBA-15 was partly destroyed. The (100) diffraction peak also disappeared after 14 d, suggesting that the ordered mesoporous structure had been lost.

For the modified S-0.01 sample, the (100), (110), and (200) diffraction peaks remained after treatment under boiling water for 7 d, implying that the order structure was maintained. The angles were shifted to higher 2θ values, which indicated a slight shrinkage of the cell dimension. Even after 14 d, the diffraction peaks were still visible. This result indicated that the hydrothermal stability of SBA-15 was improved by treating with $(NH_4)_2SiF_6$ solution.

Figure 2 shows that the unmodified SBA-15 has a typical Type IV isotherm comprising a H1-type hysteresis loop with parallel adsorption and desorption. After treatment under boiling water for 7 and 14 d, the H1-type hysteresis loop, which reflects the presence of regular arrays of the cylindrical pore structure of SBA-15, had disappeared completely. The surface area (see Table 1) also decreased from 644 to 176 and then to 107 m^2/g, and the mean pore size was reduced from 8.5 nm to 5.5 nm.

The S-0.01 sample exhibited the same H1-type hysteresis loop as the unmodified SBA-15 sample. This suggested that the treatment with the amount of $(NH_4)_2SiF_6$ used did not change the ordered structure of SBA-15. The surface area became smaller (424 m^2/g) than that of unmodified SBA-15, and the mean pore size was decreased to 7.7 nm from 8.5 nm. In the XRD result, both the (100) diffraction peaks of S-0.01 and unmodified SBA-15 samples had the same 2θ values (0.9^o), suggesting they had the same unit cell parameters. Therefore, the smaller mean pore size of the S-0.01 sample implied that the S-0.01 sample had thicker mesoporous wall after treatment with $(NH_4)_2SiF_6$. This probably resulted from the deposition of some SiO_2 on the wall. The deposition may have blocked some of the micropores of SBA-15 so that the surface area of the S-0.01 sample was decreased.

After treatment with boiling water, the S-0.01-7 sample still showed the H1-type hysteresis loop. Its surface area was as high as 375 m^2/g, which was only a decrease of 49 m^2/g compared with that before the treatment with boiling water. For the S-0.01-14 sample, the H1-type hysteresis loop showed some deformation. In the range of p/p_0 from 0.65 to 0.75, the adsorbed volume showed a sudden step, which, like the H1-type hysteresis loop, suggested the S-0.01-14 sample still contained some ordered mesoporous structure. The closed point of the hysteresis loop appeared at the higher relative pressure of $p/p_0 = 1.0$, suggesting some mesopores were destroyed to form larger pores, but its surface area was as high as 310 m^2/g, which was higher than that of the SBA-15-14 sample. The result, consistent with the XRD data, indicated clearly that SBA-15 modified with $(NH_4)_2SiF_6$ had a higher hydrothermal stability.

The S-0.01-7 and S-0.01-14 samples have the same mean pore size as the S-0.01 sample, but all the (100), (110), and (200) diffraction peaks were shifted to higher 2θ values compared to the S-0.01 sample. This meant that the mesopore walls of the S-0.01 sample were shrunk by the treatment under boiling water.

The SEM images (Fig. 3) showed that the SBA-15 sample had a ropelike morphology, and was made up of bundles of ropes. After treatment with boiling water, the bundles of ropes in the SBA-15-7 sample became loose. This phenomenon was more obvious in the SBA-15-14 sample. For the S-0.01 sample, the bundles were maintained as tightly as before the treatment under boiling water. No loosening occurred in the S-0.01-7 and S-0.01-14 samples, which showed the stabilization effect of $(NH_4)_2SiF_6$ on the structure of the SBA-15 material.

The TEM images (Fig. 4) showed that the structure of the SBA-15 sample became disordered gradually with increasing treatment time under boiling water. After 14 d, no order structure was observed in the SBA-15-14 sample. The S-0.01 sample held its ordered structure well during the treatment under boiling water. Even after 14 d, the S-0.01-14 sample still exhibited excellent order. This was in good agreement with the above XRD and nitrogen absorption results and SEM images.

2.2 Hydrothermal stability under 100% H_2O stream at 800 °C

For further investigating the stabilization effect of $(NH_4)_2SiF_6$, the S-0.01 sample was hydrothermally treated under 100% H_2O stream at 800 °C for different time.

The SAXS pattern (Fig. 5) and N_2 adsorption isotherms (Fig. 6) showed that sample S-0.01-800-12 gave well resolved (100), (110), and (200) diffraction peaks and a distorted H1-type hysteresis loop. Its ordered mesopores were seen clearly in the TEM images (Fig. 7). All these results indicated that the S-0.01 sample maintained the ordered mesoporous structure well under 100 % H_2O stream at 800 ^oC for 12 h. However, after 24 h, no pores were observed in the S-0.01-800-24 sample, suggesting the porous structure was destroyed completely.

When the SBA-15 sample was hydrothermally treated under 100% H_2O stream at 800 ^oC, its surface area declined rapidly with time for times less than 6 h. Then the curve flattened out (Fig. 8). This meant that unmodified SBA-15 was unstable. Its order structure was destroyed within 6 h under 100% H_2O stream at 800 ^oC. In contrast, the surface area of the S-0.01 sample decreased slowly and linearly with time. Its initial surface area was lower than that of SBA-15, but this became higher than that of SBA-15 sample after 3 h. This meant that the pre-treatment with $(NH_4)_2SiF_6$ prevented the structure from collapsing as fast in SBA-15. The slow damage of the ordered structure was one of the important reasons for why the modified SBA-15 has a higher hydrothermal stability.

2.3 The influence of the amount of $(NH_4)_2SiF_6$ used

The question was: since some $(NH_4)_2SiF_6$ (1% SiO_2 of SBA-15) had an obvious stabilization on the hydrothermal stability of the SBA-15 material, would more $(NH_4)_2SiF_6$ strengthen the effect? Table 2 clearly shows that the initial surface areas of the samples from S-0.01 to S-0.12, which were modified with various amounts of $(NH_4)_2SiF_6$, decreased to ~420 m^2/g, suggesting that the amount of $(NH_4)_2SiF_6$ used has little influence on the initial surface area of the modified samples. When they were treated with boiling water for 7 and 14 d, the surface areas decreased with increasing amounts of $(NH_4)_2SiF_6$ used, rather than an increase as we had expected. This indicated that more $(NH_4)_2SiF_6$ cannot promote the stabilization effect further. On the contrary, it was harmful because more F^- ions can increase their etching of the framework of SBA-15. Only sample S-0.12, for which the most amount of $(NH_4)_2SiF_6$ was used, showed promoted stability: its specific surface area remained as high as 357 and 326 m^2/g, respectively, after it was treated with boiling water for 7 and 14 d. This different influence of the $(NH_4)_2SiF_6$ amount on the hydrothermal stability of SBA-15 can be explained by the following stabilization mechanism of $(NH_4)_2SiF_6$.

2.4 The influence of F^- ions

Some F^- ions were introduced during the modification with $(NH_4)_2SiF_6$. What influence on the hydrothermal stability of SBA-15 did they have?

Table 2 shows the BET surface areas of the F-*X* series samples, which were modified with NH_4F. These were around 420 m^2/g, which were much lower than that of the SBA-15 material (644 m^2/g). This meant that F^- ions can etch the framework of SBA-15 and destroy it. The etching function of the F^- ions was also a main reason for the surface area decrease of the S-X series samples.

Sample F-0.01 has a similar initial surface area as sample S-0.01. After it was treated with boiling water for 7 and 14 d, its surface area dropped to 321 and 293 m^2/g, respectively. These were lower than that of the corresponding sample S-0.01 (375 and 310 m^2/g), but were obviously higher than that of SBA-15 (176 and 107 m^2/g). This suggested that F^- ions can improve the hydrothermal stability of SBA-15. The action of F^- ions on other ordered mesoporous silicas has been reported [29–31]. It is considered to mainly result from the exchange of surface Si-OH groups by F^- ions. Si-F bonds have high hydrophobicity and resistance to water erosion. Xu et al. [32] confirmed by ^{19}F NMR that this exchange of Si–OH groups and F^- ions existed in a AlMCM-41 mesoporous material modified with NH_4F.

As compared with sample F-0.01, sample S-0.01 showed better hydrothermal stability. This implied that the function of Si insertion, as well as the hydrophobization of F^- ions, also has an important contribution in promoting the stability.

After the treatment with 100% H_2O stream for 7 or 14 d, the surface areas of the F-*X* series samples decreased with increasing amount of NH_4F, indicating that more NH_4F did not benefit the stabilization. This phenomenon was also found in the S-*X* series samples, except for the S-0.12 sample, in which $(NH_4)_2SiF_6$ amount reached 12% SiO_2, which showed a promoted stabilization, unlike the F-0.12 sample. This difference resulted from the unusual stabilization mechanism of $(NH_4)_2SiF_6$ and NH_4F.

2.5 Stabilization mechanism of $(NH_4)_2SiF_6$

When SBA-15 was modified with $(NH_4)_2SiF_6$ and NH_4F, respectively, the hydroxyl peak intensity of samples S-*X* and F-*X* at 3734 cm^{-1} decreased slightly, and that at 3667 cm^{-1} increased a little, resulting in the hydroxyl peak widening (Fig. 9). Xiao et al [33] suggested that the change to the peak at 3667 cm^{-1} was because the silicon hydroxyl peak was affected by the hydrogen bond of nearby groups in the MCM-41 material. In the S-*X* and F-*X* series samples, the surface Si–OH groups have been exchanged by F^- ions. The negative charge of F^- ions is greater than that of OH^- ions, so the strengthening of the hydrogen-bond interaction made the peak at 3667 cm^{-1} increase slightly in intensity.

The similar hydroxyl spectra of the S-*X* and F-*X* series samples indicated that F^- ions from $(NH_4)_2SiF_6$ and NH_4F have the same effect on the SBA-15 surface. As mentioned above, F^- ions can react with Si–OH to form Si–F. If this was so, the hydroxyl peak intensities of the S-*X* and F-*X* samples should decrease gradually with the increase of F^- ions. However, Fig. 9 shows they were not reduced. This was due to two possibilities: (1) The F^- ions here were introduced by a pre-treatment, and they only react with and replace surface hydroxyl groups, but did not infiltrate into the inner wall of SBA-15. Since the amount of hydroxyl groups on the surface of SBA-15 was much less than that in the bulk, the hydroxyl spectra were little influenced by F^- ions introduced in the pre-treatment; (2) F^- ions can etch the framework of SBA-15 to form a new Q^3 ($Si(OSi)_3OH$) structure (see ^{29}Si NMR results below). This counteracted the replacement effect of F^- ions.

Figure 10 shows ^{29} Si NMR spectra of the SBA-15, S-0.01, and F-0.01 samples. Two peaks centered at δ = –101 and –110 were observed. These were attributed to silicon atoms with three siloxane bonds and one silanol group, Q^3 and with four siloxane bonds, $Si(OSi)_4$ (Q^4), respectively [34]. The ratios of Q^3/Q^4 were 4.7%, 15.7%, and 19.8%, respectively. It is clear that the peak intensity of the Q^3 peak increased when the SBA-15 material was modified with $(NH_4)_2SiF_6$ and NH_4F. This result suggested that F^- ions not only replaced surface hydroxyl groups to form a hydrophobic surface, but also etched the framework of SBA-15 to form the Q^3 structure from Q^4.

The Q^3/Q^4 ratios of the S-0.01 and F-0.01 samples were such that the value of the former was 15.7%, and less than the 19.8% of the latter although the amounts of F^- ions introduced were the same. This indicated clearly that some Si atoms have been inserted into the surface defects of the SBA-15 material to form the $Si(OSi)_4$ structure from the $Si(OSi)_3OH$ structure when SBA-15 was modified with $(NH_4)_2SiF_6$. This result proved that ammonium fluorosilicate was an effective reagent to supply Si and repair the surface defects of SBA-15.

The stabilization mechanism of $(NH_4)_2SiF_6$ on the hydrothermal stability of SBA-15 is shown in Scheme 1.

There are some terminal hydroxyl groups and crystal defects on the surface of the SBA-15 sample. When SBA-15 was treated with some $(NH_4)_2SiF_6$ (1% SiO_2, Scheme 1(a)), Si atoms can insert into the surface defects and repair them. F^- ions here have two effects: first, the replacing of surface hydroxyl groups to form a hydrophobic surface, and second, the etching of the framework to form new Q^3 crystal defects. With increasing $(NH_4)_2SiF_6$ amount (1%–12% SiO_2, Scheme 1(b)), since surface defects have already been occupied by Si atoms, the extra Si cannot penetrate into the bulk phase to repair defects there because of steric hindrance. These extra Si atoms do not improve the crystal structure and enhance the hydrothermal stability of SBA-15. To the contrary, introducing more $(NH_4)_2SiF_6$ will increase the F^- ion concentration, which would aggravate the etching effect of F^- ions and produce more unsaturated coordination Q^3 structure. Thus, the hydrothermal stability would not be as good as that achieved when modified with a small amount of $(NH_4)_2SiF_6$. With a further increase of the $(NH_4)_2SiF_6$ amount (> 12% SiO_2, Scheme 1(c)), since a large amount of SiO_2 was deposited on the wall of SBA-15 to form a dense SiO_2 protective film, which can prevent the steam from eroding the wall of the SBA-15 material, the hydrothermal stability of SBA-15 was improved.

From the above mechanism, the stabilization by $(NH_4)_2SiF_6$ on the hydrothermal stability of SBA-15 depends on the optimization of positive factors, such as silicon insertion and surface hydrophobicity of F^- ions, and the negative factor of F^- ion etching. Enhancing the positive factors and weakening the negative factor would benefit the stabilization effect of $(NH_4)_2SiF_6$, but the F/Si ratio in the $(NH_4)_2SiF_6$ molecule is fixed. When more Si sources are introduced, more F^- ions must also be introduced. This is one of the main problems of this method.

Only a small amount of $(NH_4)_2SiF_6$ (~1% SiO_2) has a very good effect on improving the hydrothermal stability of SBA-15. This method is simple, facile and cheap as compared with other methods. Furthermore, the chemical properties and catalytic performance are not changed by this modification because no heteroatoms were introduced into the SBA-15 material.

3 Conclusions

A SBA-15 material modified by a small amount of $(NH_4)_2SiF_6$ (1% SiO_2 of SBA-15) exhibited excellent and improved hydrothermal stability. It kept the ordered mesoporous structure very well when treated under boiling water for 14 d or 100% stream at 800 °C for 12 h. The BET surface areas were as high as 310 and 213 m^2/g, after these respective treatments, and much higher than that of unmodified SBA-15 sample after the same treatments. This method is simple and cheap, has low energy consumption and does not change the chemical properties of SBA-15.

Full-text paper available online at Elsevier ScienceDirect
http://www.sciencedirect.com/science/journal/18722067